Biochimica et Biophysica Acta 1853 (2015) 2055–2065

Contents lists available at ScienceDirect

Biochimica et Biophysica Acta

journal homepage: www.elsevier.com/locate/bbamcr

Structural effects of Mg^{2+} on the regulatory states of three neuronal calcium sensors operating in vertebrate phototransduction☆

Valerio Marino [a], Stefan Sulmann [b], Karl-Wilhelm Koch [b], Daniele Dell'Orco [a,c,*]

[a] Department of Life Sciences and Reproduction, Section of Biological Chemistry, University of Verona, Italy
[b] Department of Neurosciences, Biochemistry Group, University of Oldenburg, Germany
[c] Center for BioMedical Computing (CBMC), University of Verona, Italy

ARTICLE INFO

Article history:
Received 5 September 2014
Received in revised form 25 October 2014
Accepted 28 October 2014
Available online 4 November 2014

Keywords:
Phototransduction
Neuronal calcium sensor
Conformational switch
Guanylate cyclase-activating protein
Magnesium
Molecular dynamics

ABSTRACT

The effects of physiological concentration of magnesium on the switch states of the neuronal calcium sensor proteins recoverin, GCAP1 and GCAP2 were investigated. Isothermal titration calorimetry was applied for binding studies. Circular dichroism spectroscopy was used to characterize protein thermal stability, secondary and tertiary structure in conditions of high and low [Ca^{2+}], mimicking respectively the dark-adapted and light-exposed photoreceptor states during the phototransduction cascade. Further, molecular dynamics (MD) simulations were run to investigate the dynamical structural properties of GCAP1 in its activator, inhibitor and putative transitory states.

Our results confirmed that Mg^{2+} is unable to trigger the typical Ca^{2+}-induced conformational change of recoverin (myristoyl switch) while it decreases its thermal stability. Interestingly, Mg^{2+} seems to affect the conformation of GCAP2 both at high and low [Ca^{2+}], however the variations are more substantial for myristoylated GCAP2 in the absence of Ca^{2+}. GCAP1 is responsive to Mg^{2+} only in its low [Ca^{2+}] state and Mg^{2+}-GCAP1 tertiary structure slightly differs from both apo and Ca^{2+}-bound states. Finally, MD simulations suggest that the GCAP1 state harboring one Mg^{2+} ion bound to EF2 acquires structural characteristics that are thought to be relevant for the activation of the guanylate cyclase. Moreover, all the putative Mg^{2+}-bound states of myristoylated GCAP1 are structurally less flexible than Ca^{2+}-bound states. GCAP1 acquires a more compact tertiary structure that is less accessible to the solvent, thereby inducing a different conformation to the myristoyl moiety, which might be crucial for the activation of the guanylate cyclase. This article is part of a Special Issue entitled: 13th European Symposium on Calcium.

1. Introduction

Calcium (Ca^{2+}) plays a crucial role as a second messenger in rod and cone photoreceptor cells where, depending on the species, its concentration drops from ~250–800 nM to ~20–100 nM during the activation of the phototransduction cascade [1,2]. Being directly involved in negative feedback mechanisms, Ca^{2+} permits the regulation of light-sensitivity in photoreceptors and allows the typical adaption mechanisms observed under different light regimes [3–6]. Subtle changes in [Ca^{2+}] are detected by neuronal calcium sensor (NCS) proteins belonging to the EF-hand superfamily, which precisely regulate the enzymatic activity of their targets [7,8], by adopting specific conformations in response to Ca^{2+}-binding. Among NCS proteins, recoverin (Rec) exerts its regulatory properties on the activity of rhodopsin kinase by exploiting a mechanism known as myristoyl switch. Recoverin triggers from a "tense" (T), compact conformation in which, at low [Ca^{2+}] the post-translationally-bound myristoyl group is buried in a hydrophobic pocket to a more "relaxed" (R), extended conformation in which, at high [Ca^{2+}] the myristic moiety is solvent-exposed and more likely anchored to disk membranes [9,10]. Unlike Rec, the NCS guanylate cyclase-activating proteins 1 and 2 (GCAP1, GCAP2) do not undergo a myristoyl switch mechanism, but operate in a calcium-relay system [3] to make gradual responses to small changes in [Ca^{2+}], which results in a fine-tuned control of the activities of photoreceptor specific sensory membrane bound guanylate cyclases (which for reasons of simplicity we will refer in the text to a singular GC), specifically inhibiting the enzyme responsible for the synthesis of cyclic GMP (cGMP) at high [Ca^{2+}], and stimulating it at low [Ca^{2+}] [4,11].

While it is well established that Ca^{2+} plays a major role in many biochemical processes underlying the phototransduction cascade, the role of magnesium (Mg^{2+}), another divalent cation present at much

Abbreviations: Rec, recoverin; GCAP1, guanylate cyclase-activating protein 1; GCAP2, guanylate cyclase-activating protein 2; GC, membrane bound guanylate cyclase; MD, molecular dynamics; CD, circular dichroism; SASA, solvent accessible surface area; RMSD, root-mean square deviation; RMSF, root-mean square fluctuation

☆ This article is part of a Special Issue entitled: 13th European Symposium on Calcium.

* Corresponding author at: Strada le Grazie 8, 37134 Verona, Italy. Tel.: +39 045 802 7637.
E-mail address: daniele.dellorco@univr.it (D. Dell'Orco).

http://dx.doi.org/10.1016/j.bbamcr.2014.10.026
0167-4889/

higher concentration in both rod and cone outer and inner segments is less well understood. Mg^{2+} is an important cofactor for the fundamental nucleosides triphosphate ATP and GTP and a large number of enzymes appear to be regulated by Mg^{2+} in conditions that match the large physiological concentrations observed in tissues and cells [12]. In photoreceptor cells, [Mg^{2+}] stabilizes at relatively high values (~1 mM), independent of significant variations of pH, Ca^{2+} and Na^{+}, leading to the conclusion that unlike Ca^{2+} it does not participate in the dynamic regulation of phototransduction [13]. It is however known that EF-hand motifs that bind Ca^{2+} via an ideal pentagonal bipyramid geometry consisting of six oxygen atoms from carboxyl and carbonyl groups of the protein and an oxygen atom from a water molecule, may also bind Mg^{2+} in the same binding sites, though via an octahedral geometry [14]. The lack of a bidentate coordination usually provided by a Glu residue in the case of Ca^{2+} binding results in a monodentate coordination, overall leading to six rather than seven oxygen ligands in the case of Mg^{2+}. Depending on their specific affinity for Ca^{2+}, which may vary from 10^{-9} M to 10^{-6} M, Ca^{2+}-binding sites usually bind Mg^{2+} ions four to five orders of magnitude less strongly, thus making it particularly difficult to measure the dissociation constants [15]. Moreover, the radius of a hydrated Mg^{2+} ion is ~400-fold larger compared to the dehydrated one, while that of Ca^{2+} increases ~25-fold upon hydration. As a consequence, Mg^{2+} cannot be easily stripped of its hydration shell, and despite the similar chemical reactivity and charge the two cations show often very different biochemical behaviors [16]. Establishing general principles to quantify Mg^{2+} competition for Ca^{2+}-binding sites is therefore not trivial, as each binding site, and eventually each protein may behave differently, depending on the relative affinity for the cations and their local concentrations.

In the last years a number of exhaustive biochemical and biophysical investigations have revealed that free Mg^{2+} is important for the activation of GC by GCAP1. Mg^{2+} seems to bind to apo-GCAP1 with moderate affinity [17,18] and the apo form of GCAP1 seems not to exist physiologically, nor to be able to activate GC or colocalize with it in experiments with cells [19]. Previous studies on Rec suggest that Mg^{2+} does not influence the known myristoyl switch mechanism [20], but no dedicated structural study was performed so far. Finally, while a Ca^{2+}/Mg^{2+} exchange mechanism of general validity for GCAP-mediated activation of GC was proposed [21] based on the evidence that GCAP2 is also functionally affected by Mg^{2+} [17,22], to our knowledge the structural effects of Mg^{2+} on GCAP2 have never been experimentally studied so far, nor has the affinity for binding been estimated.

In this work we present a comparative analysis of the structural effects of Mg^{2+} on the regulatory states of Rec, GCAP1 and GCAP2 by focusing on conditions of high and very low Ca^{2+}, thus mimicking dark-adapted and illuminated photoreceptor cells. We measured variations of secondary and tertiary structure in different conditions, including the presence and absence of the post-translational myristoylation of the NCS proteins at the N-terminal. For myristoylated GCAP1 (mGCAP1), we performed comparative molecular dynamics simulations of the activating, inhibitory and putative transitory states, highlighting important dynamical features, which might be critical for switching between different regulatory states.

2. Material and methods

2.1. Protein expression and purification

Proteins were heterologously expressed in *Escherichia coli* and purified by hydrophobic interaction chromatography (myristoylated and non-myristoylated Rec (m/nmRec); see Refs. [23,24] for details) or by size exclusion chromatography and anion-exchange chromatography (m/nmGCAP1; see ref. [25] for details; m/nmGCAP2 see [26] for details). Protein sample purity was verified by SDS-PAGE. Protein buffer was exchanged with decalcified NH_4HCO_3, and samples were then concentrated, lyophilized and stored at −80 °C until use.

2.2. Circular dichroism spectroscopy and thermal denaturation studies

Circular dichroism (CD) spectroscopy studies were performed with a Jasco V-710 spectropolarimeter equipped with a Peltier type thermostated cell holder, using quartz cuvettes with path length of 1 cm for near UV spectra (250–320 nm) and 0.1 cm for far UV spectra (200–250 nm). Both near UV and far UV spectra were recorded at 37 °C at a scan rate of 50 nm min^{-1}, with a bandwidth of 1 nm and an integration time of 4 s. For each spectrum five accumulations were averaged and the spectrum of the buffer was recorded before each set of measurements and subtracted. For far UV spectra protein concentration was 8–10 μM for Rec, 17–20 μM for GCAP2 and 8–13 μM for GCAP1, while for near UV spectra it was respectively 15–20 μM, 40–42 μM and 26–52 μM. All experiments were performed in 5 mM Tris–HCl pH 7.5, 150 mM KCl, and 2 mM DTT.

Both far UV and near UV spectra were recorded: i) in the presence of 10-fold excess EGTA with respect to protein concentration; ii) after the addition of 1 mM $MgCl_2$ or 2-fold excess $CaCl_2$ with respect to the concentration of EGTA; and iii) after the addition of the other salt not added in the previous step. Thermal denaturation of all proteins was monitored between 20 °C and 96 °C in the same conditions as for far UV spectra, as far as protein, EGTA, $CaCl_2$ and $MgCl_2$ concentrations are concerned. The ellipticity signal at 208 nm (θ_{208}) was recorded at a scan rate of 1 °C min^{-1} and a response time of 4 s. The thermal denaturation analysis was performed assuming a two-state transition process, where the θ_{208} signal recorded as a function of temperature represents the fraction of folded and partly unfolded protein. When possible, thermal denaturation curves were fitted to a 4-parameter Hill sigmoid and a value for the melting temperature was estimated, otherwise a minimum value of transition temperature evaluation was estimated. The equation for the fitting curve was:

$$y = b_n + \frac{|b_n - b_u| T^H}{T_m^H + T^H}$$

where b_n is the baseline value (θ_{208}) of the native protein, b_u is the baseline value of the partly unfolded protein, T is the temperature, H is the Hill coefficient and T_m is the melting temperature.

2.3. Mg^{2+}-GCAP2 titrations monitored by intrinsic fluorescence spectroscopy

Protein samples were excited at 290 nm wavelength, while emission fluorescence spectra were recorded between 300 and 380 nm at 25 °C in 1 cm quartz cuvette using a Jasco FP-750 spectrofluorimeter, where the scan rate was set to 60 nm min^{-1} and excitation and emission bandwidth was set to 5 nm. Mg^{2+} buffers used for fluorescence titration experiments were prepared using 5 mM Tris–HCl pH 7.5, 150 mM KCl, 100 mM EGTA and $MgCl_2$ at variable concentrations, everything was dissolved in or diluted with the aforementioned Tris–HCl buffer. Free Mg^{2+} concentration for each titration point was calculated according to the Ca-Mg-ATP-EGTA Calculator software using NIST database (http://maxchelator.stanford.edu/CaMgATPEGTA-NIST.htm) by fixing T = 25 °C, pH = 7.5, and ionic strength = 0.15 M. By mixing these solutions, the final free Mg^{2+} concentration was varied in the 9.8 μM–29.9 mM range. Protein concentration was ~0.8 μM for each titration point. After recording three accumulations of the spectrum in the presence of 100 μM EGTA, only the intensity at the wavelength corresponding to the maximum intensity of fluorescence emission of the apo spectrum was monitored for the other titration points, which was expected to change according to Mg^{2+}-binding.

2.4. Isothermal titration calorimetry

Mg^{2+} binding to apo-GCAP2 was monitored by isothermal titration calorimetry (ITC) as described earlier [27]. In brief we used an VP-ITC instrument from Microcal (Northampton, MA, USA) at T = 25 °C, and the decalcified GCAP2 form was present in the recording cell at 3.6–14 μM concentration in the same decalcified Tris buffer (5 mM Tris–HCl pH = 7.5, 150 mM KCl) used for the CD studies. The titration was performed by subsequential injections of 3–5 μL 10 mM $MgCl_2$ into the recording cell. Remaining Ca^{2+} impurities in the decalcified Tris buffer were determined by a BAPTA absorption assay and ranged from 10 to 13 nM.

Best fitting results of the ITC data were obtained by a sequential two site binding model implemented in the Origin 7 software package (Microcal), providing apparent dissociation constants (K_D) and enthalpy changes (ΔH) upon magnesium binding.

2.5. Molecular dynamics simulations

A homology model of human mGCAP1 was built using the three-dimensional structure of chicken mGCAP1 in its Ca^{2+}-bound form as template [28], according to a procedure elucidated in a previous work [29]. All simulation states were modeled either by removing Ca^{2+} ions from each respective EF-hand binding site or by substitution with a Mg^{2+} ion, thus obtaining the states shown in Fig. 5. In particular, we prepared starting structures corresponding to: i) two GC-activating states (one Mg^{2+} ion bound to EF2, the other EF-hands accommodating no ion; indicated from now on as $EF2^{Mg^{2+}}$; another one accommodating two Mg^{2+} ions, $EF2^{Mg^{2+}}$ $EF3^{Mg^{2+}}$); ii) two possible transitory states ($EF2^{Mg^{2+}}$ $EF3^{Ca^{2+}}$ and $EF2^{Ca^{2+}}$ $EF3^{Ca^{2+}}$); iii) the GC inhibiting state ($EF2^{Ca^{2+}}$ $EF3^{Ca^{2+}}$ $EF4^{Ca^{2+}}$); and iv) two hypothetical, presumably non physiological states (apo protein and $EF2^{Mg^{2+}}$ $EF3^{Mg^{2+}}$ $EF4^{Mg^{2+}}$).

MD simulations of all seven systems were performed using GROMACS 4.6.3 simulation package [30], with the CHARMM27 all-atom force field [31,32]. CHARMM27 parameters for describing the post-translational myristoylation were generated manually, and are available upon request for academic use. Periodic Boundary Conditions (PBC) were applied using a dodecahedral box as the cell unit and choosing 12 Å as minimum distance between the protein and the box boundaries. Water model TIP3P was used to describe the solvent. Depending on the number of cations bound to the protein, a variable number of Mg^{2+} ions was added in the solvation box in order to set the concentration of Mg^{2+} ions to 1 mM and to neutralize the system, together with 29 K^+ and 29 Cl^- ions, which were added to adjust the salt concentration to 150 mM while keeping the system neutral. In detail, the systems included: 32,610 total atoms for the apo form (9853 water molecules, 6 Mg^{2+} counterions), 32,619 total atoms for $EF2^{Mg^{2+}}$ (9856 water molecules, 5 Mg^{2+} counterions), 32,622 total atoms for $EF2^{Mg^{2+}}$ $EF3^{Mg^{2+}}$ (9857 water molecules, 4 Mg^{2+} counterions), 32,622 total atoms for $EF2^{Mg^{2+}}$ $EF3^{Ca^{2+}}$ (9857 water molecules, 4 Mg^{2+} counterions), 32,628 total atoms for $EF2^{Mg^{2+}}$ $EF3^{Mg^{2+}}$ $EF4^{Mg^{2+}}$ (9859 water molecules, 3 Mg^{2+} counterions), 32,622 total atoms for $EF2^{Ca^{2+}}$ $EF3^{Ca^{2+}}$ (9857 water molecules, 4 Mg^{2+} counterions) and 32,628 total atoms for $EF2^{Ca^{2+}}$ $EF3^{Ca^{2+}}$ $EF4^{Ca^{2+}}$ (9859 water molecules, 3 Mg^{2+} counterions).

All structures were subjected to energy minimization, first with the steepest descent (F_{max} = 1000 kJ mol^{-1} nm^{-1}) and then with the conjugate gradients algorithm (F_{max} = 500 kJ mol^{-1} nm^{-1}), keeping the position of the backbone atoms and cations bound to the protein restricted in both cases. The system was then equilibrated at 310 K for 2 ns of backbone position-restrained MD simulations and then at 310 K for 2 ns of unrestricted MD simulations. V-rescale thermostat [33] was used to keep the system temperature fixed at 310 K, by using a coupling constant τ_t of 0.1 ps. The Particle Mesh Ewald (PME) [34] method was employed to calculate electrostatic interactions. Short range attractive and repulsive interactions were computed using a Lennard-Jones potential with a cutoff of 12 Å. LINCS algorithm [35] was used to constrain all but water molecules bond length, allowing for an integration time step of 2 fs by the leap-frog algorithm. After equilibration the system underwent 200 ns unrestrained isothermal-isobaric (NPT ensemble; T = 310 K, P = 1 atm) MD simulation. System pressure was set to 1 atm using the Berendsen weak coupling algorithm [36] with a coupling constant τ_p of 1 ps.

2.6. Analysis of MD trajectories

Generated MD trajectories were subjected to different analyses. The surface accessible surface area (SASA) and the root-mean square deviation (RMSD) were calculated over the 200 ns trajectory, the latter being referred to each structure after the 4 ns equilibration. The intrinsic flexibility of the system was evaluated by computing the root mean squared fluctuation (RMSF) for each amino acid, in the time frame of the simulation, defined as time averaged-RMSD:

$$RMSF_i = \sqrt{\frac{1}{T}\sum_{t_j=1}^{T}\left|r_i\left(t_j\right) - r_i^{ref}\right|^2}$$

where T is the 200 ns MD time frame and r_i (t_j) and r_i^{ref} represent the coordinates of the C_α atom of residue i at the time t_j and after 4 ns equilibration, respectively.

RMSD and RMSF analyses were applied only on alpha carbons, while the SASA was calculated on the entire protein.

All analyses were performed using Wordom software [37,38].

Smoothing of the RMSD and SASA plots as a function of time was performed with the smoothing function within the SigmaPlot 12 package, by using the running average module with 10,000 intervals averaging 2000 points each, corresponding to one tenth of the points in the original dataset. Raw data for RMSD and SASA are reported without smoothing in Supplementary Figs. S2 and S3, respectively.

Table 1
Structural and biophysical properties of Rec, GCAP1 and GCAP2 in different conditions.

Protein	Apo		Mg^{2+}		Mg^{2+} + Ca^{2+}		Ca^{2+}		Ca^{2+} + Mg^{2+}	
	$\theta_{222}/\theta_{208}$	T_m	$\theta_{222}/\theta_{208}$	T_m	$\theta_{222}/\theta_{208}$	T_m	$\theta_{222}/\theta_{208}$	T_m	$\theta_{222}/\theta_{208}$	T_m
mRec	0.77	73.1[a]	0.76	68.8	0.87	76.5	0.86	78.8[a]	0.88	76.5
nmRec	0.85	73.8[a]	0.86	68.8	0.90	86.0	0.90	79.4[a]	0.90	86.0
mGCAP1	0.88	50.1[b]	0.90	51.5	0.91	ND[c]	0.91	>70[b]	0.92	ND[c]
nmGCAP1	0.88	42.7[b]	0.91	54.5	0.92	ND[c]	0.93	>60[b]	0.91	ND[c]
mGCAP2	0.89	ND[c]	0.87	ND[c]	0.90	ND[c]	0.89	ND[c]	0.89	ND[c]
nmGCAP2	0.90	92.1	0.90	>96	0.88	ND[c]	0.86	ND[c]	0.87	ND[c]

[a] Data from ref. [39].
[b] Data from ref. [29].
[c] Fit not possible.

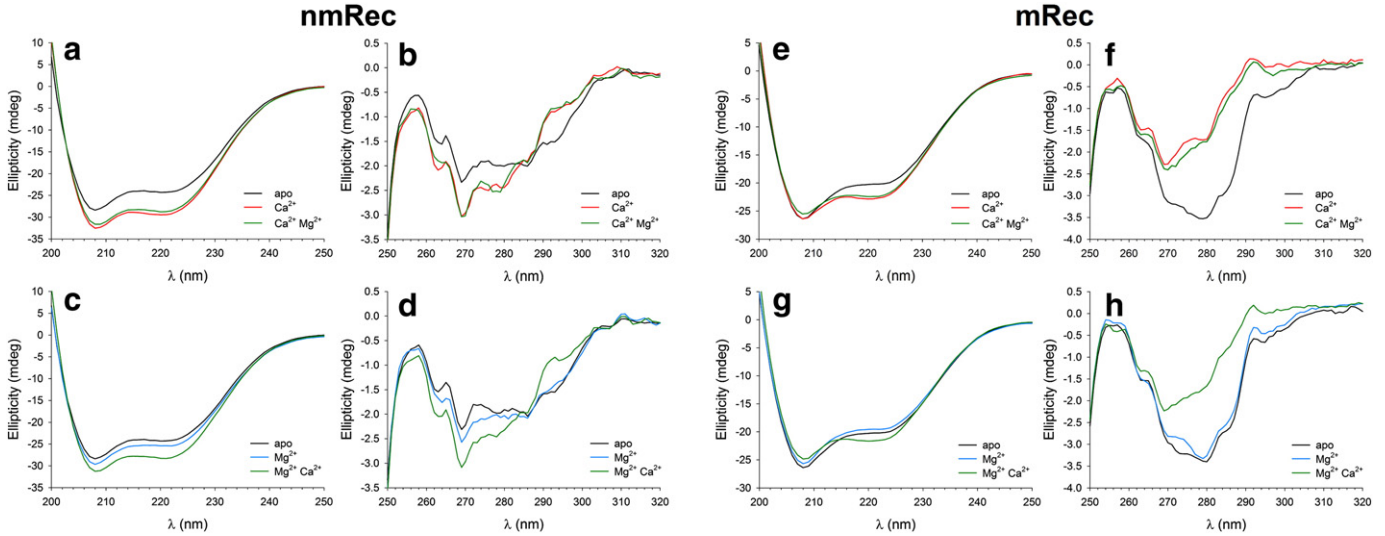

Fig. 1. Structural changes occurring in recoverin upon binding of Ca^{2+} and Mg^{2+}. All measurements were performed at T = 37 °C in 5 mM Tris–HCl pH 7.5, 150 mM KCl, 2 mM DTT buffer. (a) Far UV CD spectra of 9.8 μM nmRec in the presence of 200 μM EGTA (black), 200 μM free Ca^{2+} (red) and after addition of 1 mM Mg^{2+} (green). (b) Near UV CD spectra of 20.4 μM nmRec in the presence of 250 μM EGTA (black), 250 μM free Ca^{2+} (red) and after addition of 1 mM Mg^{2+} (green). (c) Far UV CD spectra of 9.8 μM nmRec in the presence of 200 μM EGTA (black), 1 mM Mg^{2+} (blue) and after addition of 200 μM free Ca^{2+} (green). (d) Near UV CD spectra of 20.4 μM nmRec in the presence of 250 μM EGTA (black), 1 mM Mg^{2+} (blue) and after addition of 250 μM free Ca^{2+} (green). (e) Far UV CD spectra of 8.1 μM mRec in the presence of 200 μM EGTA (black), 200 μM free Ca^{2+} (red) and after addition of 1 mM Mg^{2+} (green). (f) Near UV CD spectra of 17.2 μM mRec in the presence of 250 μM EGTA (black), 250 μM free Ca^{2+} (red) and after addition of 1 mM Mg^{2+} (green). (g) Far UV CD spectra of 8.1 μM mRec in the presence of 200 μM EGTA (black), 1 mM Mg^{2+} (blue) and after addition of 200 μM free Ca^{2+} (green). (h) Near UV CD spectra of 17.2 μM mRec in the presence of 250 μM EGTA (black), 1 mM Mg^{2+} (blue) and after addition of 250 μM free Ca^{2+} (green).

3. Results and discussion

3.1. Comparative analysis of the structural effects of Mg^{2+} on the neuronal calcium sensor proteins

In order to test whether the sequence of binding events of the different cations (Ca^{2+} and/or Mg^{2+}) matters for achieving the specific protein structures, for all three NCS proteins analyzed and both for their myristoylated and non-myristoylated forms we recorded CD spectra in the far and in the near UV after each of the following steps: i) starting from the apo protein (saturating [EGTA]); ii) addition of either 1 mM Mg^{2+} or saturating Ca^{2+}; and iii) inverting the order of the cation additions described in the previous point. Results are reported in the following figures, while a summary of the results obtained for far UV spectroscopy and thermal stability is reported in Table 1.

3.2. Effects of Mg^{2+} on the secondary and tertiary structure of Rec and on its thermal stability

The addition of saturating Ca^{2+} to apo-nmRec caused a typical increase in ellipticity (more negative signal, Fig. 1a), which was observed in earlier studies [39]. When Mg^{2+} was added to nmRec after Ca^{2+} saturation, a slight decrease in ellipticity was observed in the far UV (Fig. 1a), but no significant change was observed in protein tertiary structure, as demonstrated by the substantially overlapped spectra in the near UV region (compare green and red curves in Fig. 1b), which describe the local asymmetric environment of aromatic residues known to be especially sensitive to protein tertiary structure.

Interestingly, when $Mg^{2+}$was added to apo-nmRec, a significant increase in ellipticity was observed both in the far (Fig. 1c) and in the near UV spectra (Fig. 1d), especially in the dichroic bands of Phe and Tyr residues, suggesting that the protein might bind Mg^{2+} in these conditions. However, when Ca^{2+} was added on the top ($Mg^{2+}+Ca^{2+}$), the spectra became undistinguishable from the ones obtained in the reverse order (compare green lines in Fig. 1b and d).

Thermal denaturation studies showed that the Mg^{2+}-bound form of nmRec in the absence of Ca^{2+} is less stable than the apo form (T_m^{apo} = 73.8 °C; $T_m^{Mg^{2+}}$ = 68.8 °C; see Fig. S1 and Table 1). However, when Ca^{2+} was added at a saturating level after previous incubation with Mg^{2+}, we observed an increase in stability with respect to the one in the presence of saturating Ca^{2+} only ($T_m^{Mg^{2+}/Ca2+}$ = 86.0 °C, $T_m^{Ca^{2+}}$ = 79.4 °C, Table 1). Therefore, the structural effect of Mg^{2+} on nmRec is mostly a mild destabilization of the apo form but a major stabilization of the Ca^{2+}-bound form.

We observed some similar behavior for the myristoylated form of Rec (mRec) (Fig. 1, Table 1). Indeed, the spectral properties of mRec appeared to be only slightly affected by Mg^{2+}, both when starting from the apo and the Ca^{2+}-saturated form. Fig. 1e and g shows that the overall effect of Mg^{2+} is dampening the intensity of both the apo and Ca^{2+}-bound CD spectra in the far UV, but no significant perturbation of the spectral shape was observed either in the far or near UV (Table 1), indicative of an overall good preservation of both the secondary and the tertiary structure. In line with these structural findings, Mg^{2+} destabilized both apo and Ca^{2+}-bound mRec, with a more prominent effect on the apo form (T_m^{apo} = 73.1 °C; $T_m^{Mg^{2+}}$ = 68.8 °C; $T_m^{Ca^{2+}}$ = 78.8 °C; $T_m^{Mg^{2+}/Ca2+}$ = 76.5 °C, see Table 1).

In conclusion, these observations are in line with previous work [20] showing that Mg^{2+} may bind Rec, but it does not trigger the conformational switch, probably because the monodentate, six-coordinate structure of Mg^{2+}-bound EF-hands in the protein does not allow the myristic moiety to move out of the hydrophobic cleft where it is buried.

3.3. Effects of Mg^{2+} on the secondary and tertiary structure of GCAP1 and on its thermal stability

While the main effect of Mg^{2+} on the far UV CD spectra of Ca^{2+}-bound nmGCAP1 was a mild dampening in the intensity of the spectrum (Fig. 2a), apo-nmGCAP1 far UV spectra showed appreciable changes upon Mg^{2+} binding (Fig. 2c and Table 1), consistent with slight changes in the secondary structure or protein compactness. The molar ratio $\theta_{222}/\theta_{208}$, which describes quantitatively the spectral shape of all-α helix proteins, indeed increased from 0.88 to 0.91 (Table 1). Interestingly, while the $\theta_{222}/\theta_{208}$ ratio in the presence of both Mg^{2+} and Ca^{2+} substantially did not depend on the order by which the incubation was performed, the Ca^{2+}-bound form in the absence of Mg^{2+} showed a ratio (0.93) slightly higher than all other cases (Table 1). Near UV

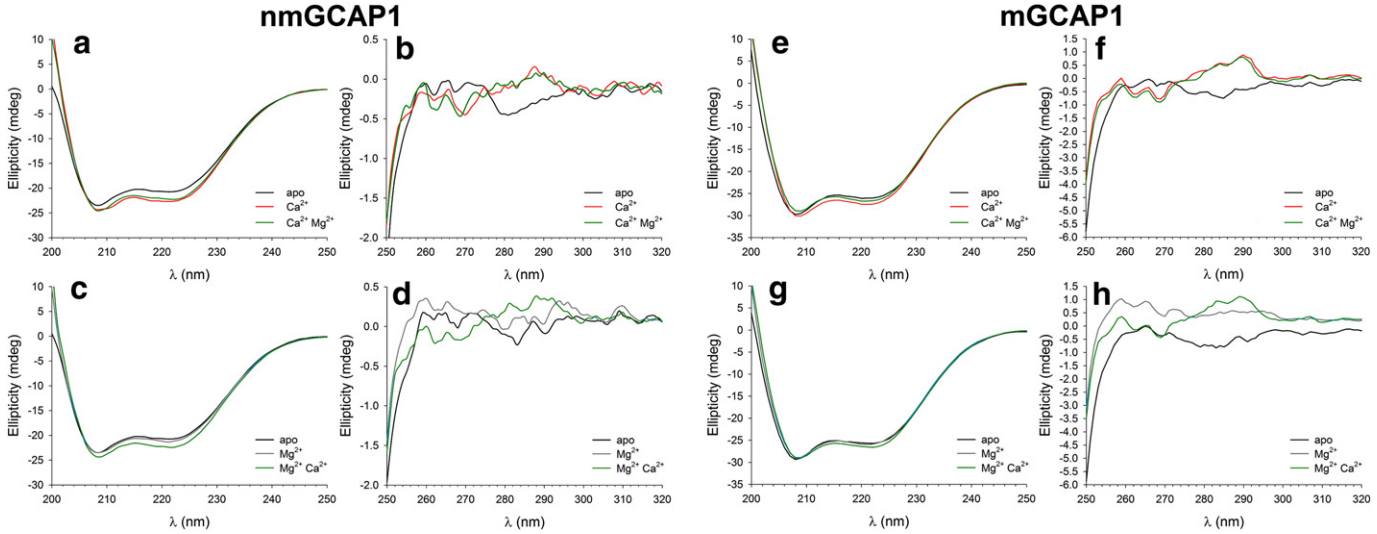

Fig. 2. Structural changes occurring in GCAP1 upon binding of Ca^{2+} and Mg^{2+}. All measurements were performed at T = 37 °C in 5 mM Tris–HCl pH 7.5, 150 mM KCl, 2 mM DTT buffer. (a) Far UV CD spectra of 13 μM nmGCAP1 in the presence of 200 μM EGTA (black), 400 μM free Ca^{2+} (red) and after addition of 1 mM Mg^{2+} (green). (b) Near UV CD spectra of 52 μM nmGCAP1 in the presence of 625 μM EGTA (black), 1.35 mM free Ca^{2+} (red) and after addition of 1 mM Mg^{2+} (green). (c) Far UV CD spectra of 13 μM nmGCAP1 in the presence of 200 μM EGTA (black), 1 mM Mg^{2+} (blue) and after addition of 400 μM free Ca^{2+} (green). (d) Near UV CD spectra of 52 μM nmGCAP1 in the presence of 625 μM EGTA (black), 1 mM Mg^{2+} (blue) and after addition of 1.35 mM free Ca^{2+} (green). (e) Far UV CD spectra of 13 μM mGCAP1 in the presence of 200 μM EGTA (black), 200 μM free Ca^{2+} (red) and after addition of 1 mM Mg^{2+} (green). (f) Near UV CD spectra of 26 μM mGCAP1 in the presence of 400 μM EGTA (black), 400 μM free Ca^{2+} (red) and after addition of 1 mM Mg^{2+} (green). (g) Far UV CD spectra of 13 μM mGCAP1 in the presence of 200 μM EGTA (black), 1 mM Mg^{2+} (blue) and after addition of 200 μM free Ca^{2+} (green). (h) Near UV CD spectra of 26 μM mGCAP1 in the presence of 400 μM EGTA (black), 1 mM Mg^{2+} (blue) and after addition of 400 μM free Ca^{2+} (green).

spectra of Ca^{2+}-bound nmGCAP1 showed only very minor variations upon the addition of Mg^{2+} (Fig. 2b), in particular in the fine structure of the Phe region, which could however be attributed to instabilities of the signal due to protein flexibility.

Interestingly, in line with what we observed for the secondary structure, binding of Mg^{2+} to apo-nmGCAP1 caused more pronounced alterations of the near UV CD spectra, extending from the Phe to the Trp bands (Fig. 2d). Upon the addition of saturating Ca^{2+} however, the spectrum became almost undistinguishable from the one obtained the other way around (adding Mg^{2+} first and then saturating with Ca^{2+}; compare green curves in Fig. 2b and d). In conclusion, in the apo form of nmGCAP1 or at conditions of very low Ca^{2+}, Mg^{2+} affects both the secondary and the tertiary structure, but it has substantially no effect on the Ca^{2+}-bound form. This also reflects on the increased thermal stability of the Mg^{2+}-bound form of nmGCAP1 versus the apo form ($T_m^{apo} = 42.7$, $T_m^{Mg^{2+}} = 54.5$, Table 1), substantially in line with what was determined by Lim et al. with differential scanning calorimetry [18]. No estimate of $T_m^{Mg^{2+}/Ca2+}$ was possible from the thermal denaturation curves (see Fig. S1), as the denaturation profile was apparently monotonic up to ~90 °C.

A slightly different situation was observed for mGCAP1. The addition of 1 mM Mg^{2+} to Ca^{2+}-saturated mGCAP1 resulted in a significant

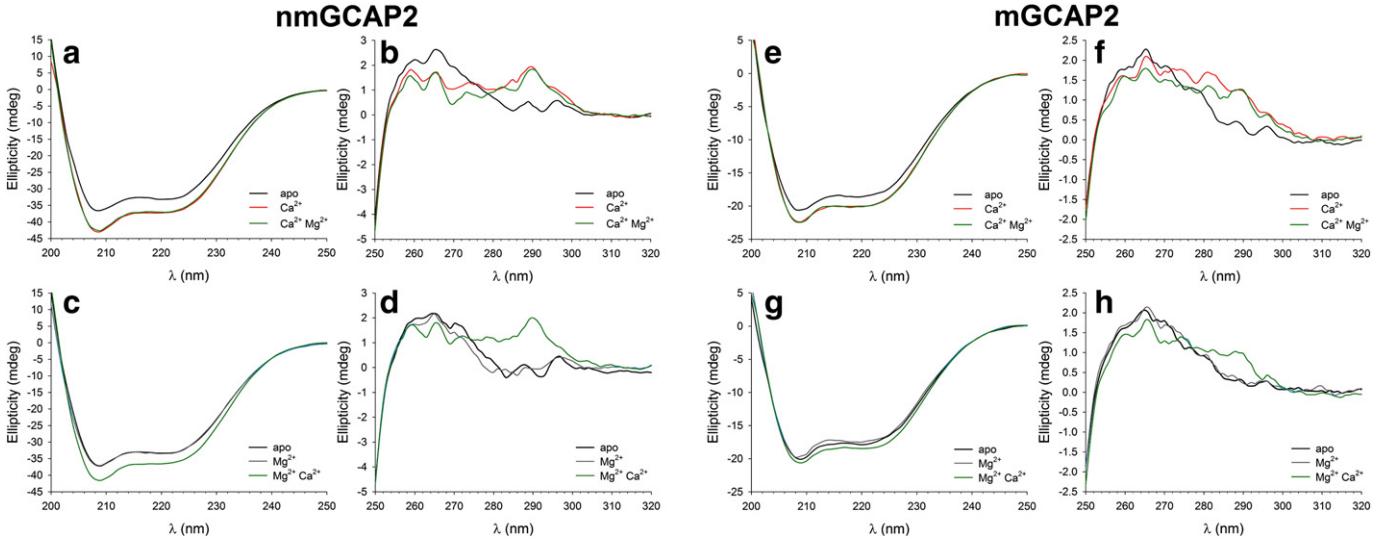

Fig. 3. Structural changes occurring in GCAP2 upon binding of Ca^{2+} and Mg^{2+}. All measurements were performed at T = 37 °C in 5 mM Tris–HCl pH 7.5, 150 mM KCl, 2 mM DTT buffer. (a) Far UV CD spectra of 19 μM nmGCAP2 in the presence of 300 μM EGTA (black), 300 μM free Ca^{2+} (red) and after addition of 1 mM Mg^{2+} (green). (b) Near UV CD spectra of 42 μM nmGCAP2 in the presence of 600 μM EGTA (black), 1.4 mM free Ca^{2+} (red) and after addition of 1 mM Mg^{2+} (green). (c) Far UV CD spectra of 19 μM nmGCAP2 in the presence of 300 μM EGTA (black), 1 mM Mg^{2+} (blue) and after addition of 300 μM free Ca^{2+} (green). (d) Near UV CD spectra of 42 μM nmGCAP2 in the presence of 600 μM EGTA (black), 1 mM Mg^{2+} (blue) and after addition of 1.4 mM free Ca^{2+} (green). (e) Far UV CD spectra of 19 μM mGCAP2 in the presence of 300 μM EGTA (black), 300 μM free Ca^{2+} (red) and after addition of 1 mM Mg^{2+} (green). (f) Near UV CD spectra of 42 μM mGCAP2 in the presence of 600 μM EGTA (black), 1.4 mM free Ca^{2+} (red) and after addition of 1 mM Mg^{2+} (green). (g) Far UV CD spectra of 19 μM mGCAP2 in the presence of 300 μM EGTA (black), 1 mM Mg^{2+} (blue) and after addition of 300 μM free Ca^{2+} (green). (h) Near UV CD spectra of 42 μM mGCAP2 in the presence of 600 μM EGTA (black), 1 mM Mg^{2+} (blue) and after addition of 1.4 mM free Ca^{2+} (green).

dampening of the far UV CD spectra (Fig. 1e), but the spectral shape did not change significantly ($\theta_{222}/\theta_{208}$ = 0.91 versus 0.92, Table 1). In line with this observation, in the near UV range the addition of Mg^{2+} did not affect at all the spectral properties of Ca^{2+}-saturated mGCAP1 in any of the typical aromatic bands (Fig. 1f).

When Mg^{2+} was added to apo-mGCAP1, the intensity of the spectrum did not significantly change, although the shape changed in a similar manner compared to the non-myristoylated form (Table 1). Spectral alterations were observed also in the near UV range (Fig. 1h), especially in the Tyr and partially in the Trp band. However, also for mGCAP1 the spectra obtained by adding first Ca^{2+} and then Mg^{2+}, or the other way around were substantially indistinguishable from one another (compare green curves in Fig. 2f and h). Thus, at high Ca^{2+} the presence of Mg^{2+} does not influence the structural properties of either the myristoylated and non-myristoylated forms of GCAP1.

The presence of Mg^{2+} slightly stabilized mGCAP1 secondary structure (T_m^{apo} = 50.1 °C, $T_m^{Mg^{2+}}$ = 51.5 °C, Table 1), but no conclusion could be drawn as to the comparison between the Ca^{2+}-bound form and the same in the presence of Mg^{2+}, since both transitions were not complete at 95 °C (Fig. S1, Table 1: $T_m^{Ca^{2+}} > 70$, $T_m^{Mg^{2+}/Ca^{2+}} > 70$ °C).

3.4. Effects of Mg^{2+} on the secondary and tertiary structure of GCAP2 and on its thermal stability

The structural behavior of nmGCAP2 in the presence of physiological Mg^{2+} significantly differed from that observed with GCAP1. No difference was detected in intensity and shape of the far UV CD spectra when Mg^{2+} was added to the apo-nmGCAP2 (Fig. 3c) or to the Ca^{2+}-saturated form (Fig. 3a), which is reflected by the identical $\theta_{222}/\theta_{208}$ ratios in the two cases (0.90 and 0.86, respectively; see Table 1). This might suggest that no Mg^{2+}-binding occurs. However, the presence of Mg^{2+} slightly influenced the environment of aromatic residues, both with or without Ca^{2+}-saturating levels (Fig. 3b and d), as proven by small but significant alterations of the near UV fine spectra. Surprisingly, the effect was more apparent when Mg^{2+} was added after Ca^{2+}-saturating levels (Fig. 3b), where differences could be appreciated in the Phe and Tyr bands.

From the analysis of thermal denaturation curves it was not possible to assess a value for the melting temperature for any of the tested case, since no transition apparently occurred at T < 96 °C (Fig. S1).

Similar to what we observed for the non-myristoylated form, addition of Mg^{2+} to the Ca^{2+}-saturated mGCAP2 did not perturb its secondary structure, as demonstrated by the overlapped far UV CD spectra (Fig. 3e, compare green and red curves), which was quantitatively confirmed by the identical (0.89) $\theta_{222}/\theta_{208}$ ratios (Table 1). Also in this case however, the tertiary structure appeared to be somewhat sensitive to Mg^{2+}, even after saturation with Ca^{2+} (Fig. 3f), as indicated by spectral changes and a decrease in intensity of the dichroic bands of Phe and Tyr residues. Interestingly and at odds with the non-myristoylated form, Mg^{2+} slightly perturbed the far UV CD spectrum of apo-mGCAP2 (Fig. 3g), with the $\theta_{222}/\theta_{208}$ ratios shifting from 0.89 to 0.87 (Table 1), but adding saturating Ca^{2+} restored the original spectral shape and intensity (Fig. 3g and Table 1; compare green curves in Fig. 3e and g). However, the tertiary structure resulted to be far less affected by Mg^{2+} when starting from the apo form of mGCAP2 (Fig. 3h), and saturating with Ca^{2+} restored a similar $Ca^{2+} + Mg^{2+}$ spectrum (see Fig. 3f for comparison). Also for mGCAP2, no clear conclusion as to the role of Mg^{2+} in stabilizing each structural state could be drawn from the analysis of thermal denaturation profiles because no transition was visible in any case (Fig. S1). The only appreciable difference was the thermal denaturation profile of mGCAP2 in the sole presence of Mg^{2+}, which compared to the non-myristoylated form, seems to start a transition earlier, thus suggesting a lower thermal stability (Fig. S1).

In conclusion, results from CD spectroscopy for m/nmGCAP2 significantly differ from those for GCAP1 and suggest that Mg^{2+} might bind to GCAP2 with different affinity and/or dynamics than it does to GCAP1. The binding might however be specific for different activation states of the calcium sensor. In particular, we could observe the following: i) for nmGCAP2, if the binding occurred, it would affect only the local environment of its aromatic residues, mostly and surprisingly at high [Ca^{2+}]; ii) for mGCAP2, results from far UV CD suggest that the binding might occur in the condition of low Ca^{2+}, however this would leave the tertiary structure substantially unperturbed; and iii) for mGCAP2, results from near UV CD suggest that the local environment of its aromatic residues is influenced by physiological Mg^{2+} even after saturation with Ca^{2+}.

While the conclusions from our CD spectroscopy analysis of GCAP1 are substantially in line with what is known as to the role of Mg^{2+} interacting with the NCS, and are compatible with defined structural consequences of a pure binding process, results for GCAP2 seem intrinsically hard to interpret, and somewhat contradictory. Overall, the data are not feasible for an interpretation based on a pure binding process, and in fact they raise some questions. Is GCAP2 binding Mg^{2+} depending on the presence of the myristoyl moiety? Does the putative binding occur even in the presence of saturating Ca^{2+}, thus presumably in other binding sites than those highly specific for Ca^{2+}? We tried to answer some of these questions by further focusing on the putative interaction of GCAP2 with Mg^{2+}.

3.5. Biophysical studies of the interaction between myristoylated/non-myristoylated GCAP2 and Mg^{2+}

In order to quantitatively investigate the binding of Mg^{2+} to GCAP2, we performed ITC experiments starting from conditions of carefully decalcified proteins and buffers. While for nmGCAP2 the pattern of heat pulses observed in all the titration experiments was incompatible with a binding process (results not shown), only in 4 out of 15 experiments performed with mGCAP2 the observed pattern was

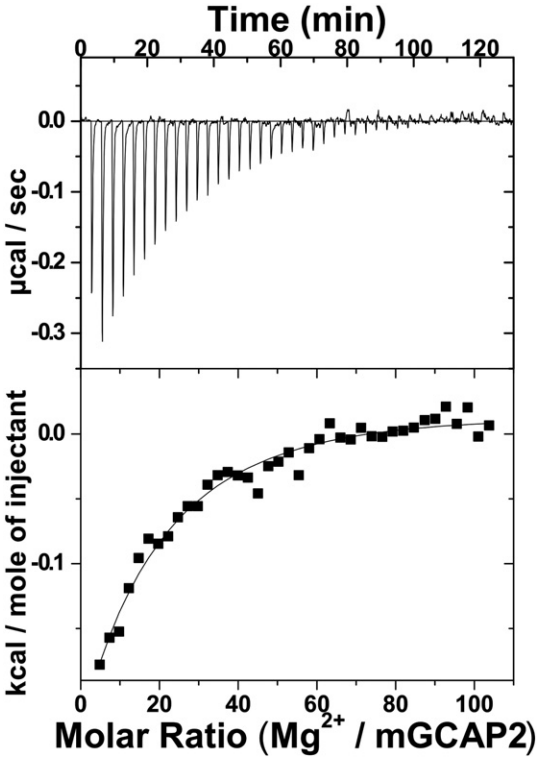

Fig. 4. Example of Mg^{2+}-mGCAP2 binding curve monitored by ITC. The upper part shows the heat pulse obtained by the injection 5 µL 10 mM $MgCl_2$ in 14 µM mGCAP2 in decalcified Tris buffer. The lower part displays the resulting enthalpy change as a function of the molar ratio of Mg^{2+} and mGCAP2 and the fitting curve.

Table 2
Thermodynamic parameters for Mg^{2+} binding to mGCAP2.

K_D^1/mM	K_D^2/mM	ΔH^1/kcal mol^{-1}	ΔH^2/kcal mol^{-1}
0.32 ± 0.20	4.4 ± 2.3	−4.6 ± 3.5	−2.7 ± 35.6

ascribable to a binding process. An example of successful titration is reported in Fig. 4, and a summary of the obtained thermodynamic parameters is shown in Table 2. Fitting the data to a sequential two-site binding model led to a physiologically relevant affinity (320 μM) for the first binding site and a non-physiological (4.4 mM) affinity for the second, lowest affinity binding site, similarly to what has been previously obtained by Lim et al. [18] for GCAP1. While the four successful titrations were per se reproducible and compatible with an exothermic process, we stress that in the majority of the other cases and in spite of the same experimental conditions and protein samples used in repeated experiments, no specific binding pattern could be obtained, thus pointing to a phenomenon that might be intrinsically poorly reproducible. Indeed, when we tried an alternative approach to detect Mg^{2+} binding to GCAP2 by performing titration experiments using the intrinsic Trp fluorescence of the protein with the same setup previously used for GCAP1 [17], we could neither observe a reproducible pattern for mGCAP2 nor for nmGCAP2 (results not shown).

Overall, our results clearly showed that the structural effects of Mg^{2+} on GCAP2 and the binding mode significantly differ from what has been so far observed for GCAP1. In particular, under the tested conditions it has been especially difficult to measure binding constants for Mg^{2+}, as some other process not occurring for GCAP1 seems to interfere with the putative binding of Mg^{2+}. One possibility to explain our data is that GCAP2 may be dimeric independent of the Ca^{2+} levels [40]. In particular, the observation that in the apo form GCAP2 is more flexible [40] may explain, at least partly, why the observed changes in far UV CD spectra (Fig. 3g) could be ascribed to the binding of Mg^{2+}. However, it could well be that even slight changes in the amount of cations as well as in protein concentration lead to different populations of monomers vs. dimers, which would complicate the interpretation of ITC and fluorescence data. Another possible phenomenon interfering with our titration experiments could be the different behavior of the myristoyl moiety in mGCAP2. Like in GCAP1, the acylic group does not extrude totally in a myristoyl switch fashion [41], however and at odds with GCAP1 it seems to be rather exposed to the solvent in both apo and Ca^{2+} states [42] and more sensitive to the external environment, as seen in experiments with membranes and micelles [43]. This could also partially contribute to the complex behavior observed in our experiments.

3.6. Molecular dynamics simulations of different regulatory states of myristoylated GCAP1

3.6.1. Diverse GC activating and inhibitory states of mGCAP1

While it is generally established that the fully Ca^{2+}-loaded state of GCAP1 is responsible for the maximal inhibition of the GC target, several recent lines of evidence showed that, when Ca^{2+} concentration drops to lower values (20–50 nM) as a consequence of photoreceptor illumination, it is a specific Mg^{2+}-bound form of GCAP1 rather than its apo state, that triggers the activation of GC [17,19,21]. In different studies, Peshenko et al. measured by fluorescence spectroscopy a moderate affinity of GCAP1 for Mg^{2+} (~0.25 mM), which was shown not to depend significantly on the presence of myristoylation [17,44]. The binding was also confirmed by ITC experiments performed by the same authors, although the detected affinity for the only physiologically relevant binding constant was lower (~0.7 mM) [18]. These quantitative data confer reliability to the hypothesis that, at least one EF-hand in GCAP1 may be occupied by Mg^{2+}, when [Ca^{2+}] is significantly low. By means of exhaustive mutational analysis and functional assays the same group demonstrated that the metal-free state of EF3, supposedly

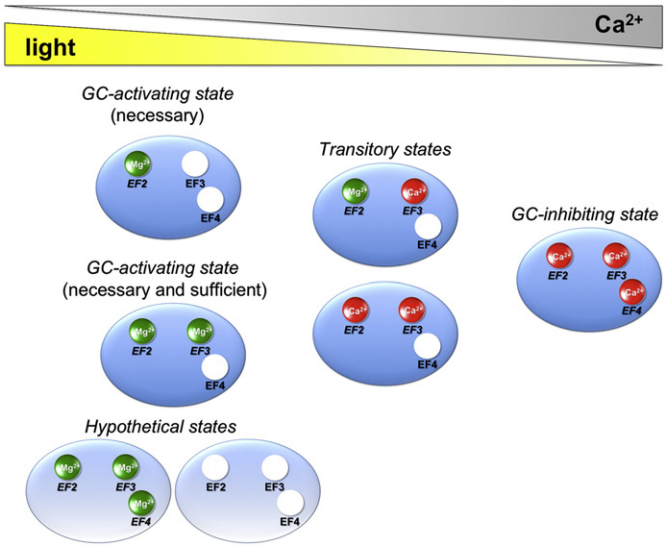

Fig. 5. Regulatory states of mGCAP1 simulated in 200 ns molecular dynamics simulations. Each of the cation-binding EF-hand is indicated. Writing in italics refers to a binding site occupied by either a Ca^{2+} (red sphere) or Mg^{2+} (green sphere) ion. The schematic positioning of each state refers to the light conditions and the relative intracellular levels of Ca^{2+}, represented at the top of the figure.

the lower affinity binding site for Mg^{2+}, reduced the efficiency of GC binding and activation, thus leading to the conclusion that the binding of a cation to EF3 seems necessary for reaching the proper functional state of the target enzyme [19,45].

By making use of the knowledge arising from these previous studies we set up 200 ns MD simulations of mGCAP1 in seven different states, reported in Fig. 5. We simulated the states corresponding to low [Ca^{2+}] and light-exposed conditions, where EF2 is necessarily occupied by Mg^{2+}, which was predicted to be bound to EF3 as well in order to activate the GC efficiently [21]. We also simulated the dark-adapted state that inhibits GC, in which EF2, EF3 and EF4 are all occupied by Ca^{2+} [21] and built models for intermediate, transitory states, in which Ca^{2+} has dissociated from the lowest affinity site EF4, and EF2 is either still occupied by a Ca^{2+} or a Mg^{2+} ion. Finally, for the sake of comparison of structure dynamics, we simulated two putative states: one in which no EF-hand is occupied by any cation (apo), and the other one where all three EF-hands are ideally occupied by Mg^{2+} ions. Neither of these states is likely to be physiologically relevant, as in the first case it was demonstrated by comprehensive mutagenesis experiments that GCAP1 mutants that do not bind Ca^{2+} and Mg^{2+} are incapable of activating GC [46]; on the other hand, the rather low affinity of GCAP1 for Mg^{2+} compared to the ~1 mM intracellular concentration together with the competition for Ca^{2+} makes it rather unlikely that more than two binding sites are ever occupied by Mg^{2+} even in the total absence of Ca^{2+}.

In the following paragraphs, we shall present the results of MD simulations of diverse GCAP1 states by first comparing the structure of each state after 4 ns equilibration with that of the apo form, in which no EF-hand is occupied by any cation, and then describing the structural features observed in the 200 ns MD production phase.

3.6.2. General structural properties of mGCAP1 states after equilibration

The comparison of seven mGCAP1 states before the production phase of MD simulations confirmed that important structural differences that distinguish specific states with respect to the putative apo form already manifest in the equilibration phase. As a clarifying example, Fig. 6 reports on the comparison between the equilibrated structures (after 4 ns) of apo-mGCAP1 and the fully Ca^{2+}-loaded state $EF2^{Ca2+}$ $EF3^{Ca2+}$ $EF4^{Ca2+}$ (holo). In apo-mGCAP1 all EF-hands were in an "open" conformation, resulting in an overall higher accessibility to

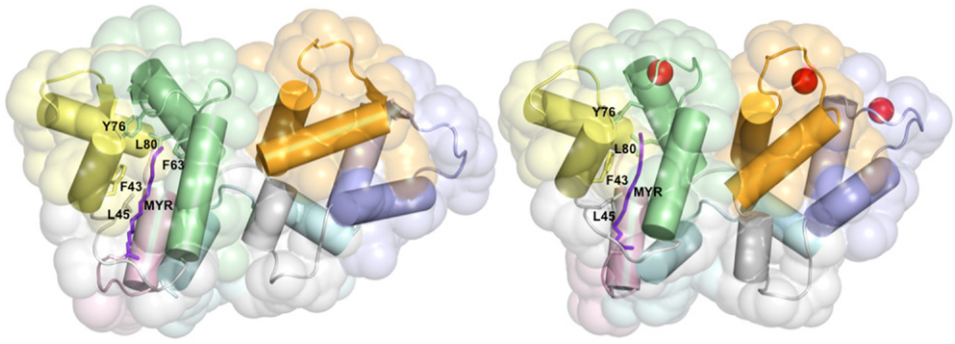

Fig. 6. Cartoon structural model of mGCAP1 in the apo form (left), and in the fully Ca^{2+}-loaded form (right) after 4 ns equilibration in all-atom MD simulations. The EF1 motive is yellow, EF2 green, EF3 orange and EF4 violet blue. Loops interconnecting EF-hand motifs are colored gray, while the N-term and the C-term are colored pale pink and pale cyan, respectively. The myristoyl moiety is represented by purple sticks. The main residues interacting with myristoyl are also represented by sticks, labeled and colored according to the structural elements they belong to. The SASA, shown in transparency, is 10,606 Å^2 for the apo form and 10,043 Å^2 for the Ca^{2+}-bound form.

the solvent as compared to the holo-mGCAP1. The fully Ca^{2+}-loaded state appeared indeed more compact already at the beginning of the MD production phase. After the equilibration phase, the myristoyl group in apo-mGCAP1 was bent at C5, to tighten the interaction with key hydrophobic residues, among which Phe 43, Leu 45, Phe 63 and Leu 80, and marginally Tyr 76. A similar bent conformation was observed for the myristic group in holo-mGCAP1, although the motion of the N-terminal loop toward the protein interior in the holo form significantly reduced the interaction with Phe 63, while maintaining the other hydrophobic interactions substantially unaltered (Fig. 6).

3.6.3. Structural dynamics of putative GC-activating states over 200 ns simulations

The 119–132 loop interconnecting EF3 with EF4 (represented in gray in Fig. 6) was generally highly flexible in the tested states, as reflected by the high RMSF values found for this structural region over 200 ns (Fig. 7b). Moreover, in some of the tested states the 120–125 strand of this loop acquired a local α-helix conformation, which showed a transient behavior. In contrast to other states however, in the apo-mGCAP1 the loop was found to be rather stable and the local helix conformation persisted over the 200 ns simulation. Another peculiar feature of the apo state was a conserved pair of H-bonds between the backbone groups NH of Ile 107 and C═O of Leu 151 and NH of Leu 153 and C═O of Gly 105, which created a short antiparallel β-sheet stable during the 200 ns simulation, which contributed to maintain EF3 and EF4 in an open conformation. Interestingly, both residues Ile 107 and Leu 151 have been found to be mutated respectively in Thr and Phe in patients suffering from cone dystrophy [47,48]. Another similarly short β-sheet was observed between EF1 and EF2, which however was not stable during the production phase. The hydrophobic interactions stabilizing the myristoyl moiety were generally conserved. When all the EF-hands were virtually occupied by a Mg^{2+} ion ($EF2^{Mg^{2+}}$ $EF3^{Mg^{2+}}$ $EF4^{Mg^{2+}}$) the C_α-RMSD calculated with respect to the apo form after the 4 ns equilibration was 3.4 Å, the highest in the whole series of GCAP1 simulated states. An apparent difference was the kink of the myristoyl group at C10, due to the hydrophobic interaction with Leu 80, but structural differences were generally spread over the whole tertiary structure, especially at the EF3 motif and 119–132 loop. Overall the $EF2^{Mg^{2+}}$ $EF3^{Mg^{2+}}$ $EF4^{Mg^{2+}}$ form was the most dynamically compact one in the series, as clearly shown by the lowest SASA profile (Fig. 7 and Fig. S3). After the first 50 ns dynamics production the structure was significantly stable, and even the highly dynamic 119–132 loop showed only minor rearrangement as compared to other cases. With respect to the equilibrated structure, main differences concerned only the EF3 loop and the conformation of the myristoyl moiety, likely due to an outward rigid displacement of the C-terminal helix.

3.6.4. Structural dynamics of more realistic GC-activating states over 200 ns simulations

The structure of mGCAP1 with one Mg^{2+} bound to EF2 ($EF2^{Mg^{2+}}$) after equilibration was significantly different from the apo form, with a C_α-RMSD of 2.8 Å. The EF2 loop (64–76), which was in an open conformation in the apo form, became now properly closed to bind a Mg^{2+} cation. The myristoyl group was still involved in interactions with Phe 43 and Leu 45 with the same orientation as in the apo form, while Phe 63 acquired a different conformation, resulting in a weaker interaction, similar to what was observed for the holo form. New stabilizing interactions involved Val 83 and Leu 176. The main structural difference with apo-mGCAP1 in the N-term domain was a different inclination and orientation of the entering helix (helix E) in the EF2 motif. Significant variations were observed also in the C-term domain, where helices had generally undergone rigid motions and the 119–132 loop showed a significantly different conformation.

During the course of the 200 ns simulation the structure of $EF2^{Mg^{2+}}$ mGCAP1 was overall fairly stable when compared to all other GCAP1 states, which is reflected by the stable and lowest C_α-RMSD profile (Fig. 7a). Even the 119–132 region was rather stable, as shown in Fig. 7b. The most flexible region was the 142–148 stretch (Fig. 7b), which corresponds to the E-helix and the loop of EF4. The formation of the transient helix in the 119–132 loop connecting EF3 and EF4 was also observed. Interestingly, due to the fact that residues 2–8 (N-terminus) tend to close toward the protein core, in line with the decrease in the overall SASA (Fig. 7c) the myristic moiety became kinked at the level of C4, acquiring a novel L-shaped conformation that was fairly stable in the simulated time course. Overall, the SASA profile confirmed that after approximately 40 ns the $EF2^{Mg^{2+}}$ mGCAP1 structure, like all the other Mg^{2+}-only-bound cases, acquired an overall conformation less solvent-exposed compared to the tested Ca^{2+}-bound forms (Fig. 7c).

The other mGCAP1 state hypothesized to be relevant for GC activation, in which two Mg^{2+} ions are bound respectively to EF2 and EF3 ($EF2^{Mg^{2+}}$ $EF3^{Mg^{2+}}$) showed a 3.2 Å C_α-RMSD compared to apo mGCAP1, which became 1.9 Å when compared to $EF2^{Mg^{2+}}$. Comparison with the $EF2^{Mg^{2+}}$ state highlighted, as the main difference, a higher flexibility of the 119–132 region in the time course of the 200 ns-simulation (Fig. 7b), otherwise a rather similar conformation was observed. In line with what was observed in the $EF2^{Mg^{2+}}$ form, the SASA stabilized after ~80 ns to an average value that was lower compared to the Ca^{2+}-bound forms. The acyl chain of the myristoyl group in some of the frames kinked around C7 and was stabilized by interactions with Phe 63, Trp 21 and Val 83. Moreover, the simulation showed a rotation of the myristoyl group around C1 leading to an L-shaped conformation, which was however significantly less stable than the one observed for $EF2^{Mg^{2+}}$.

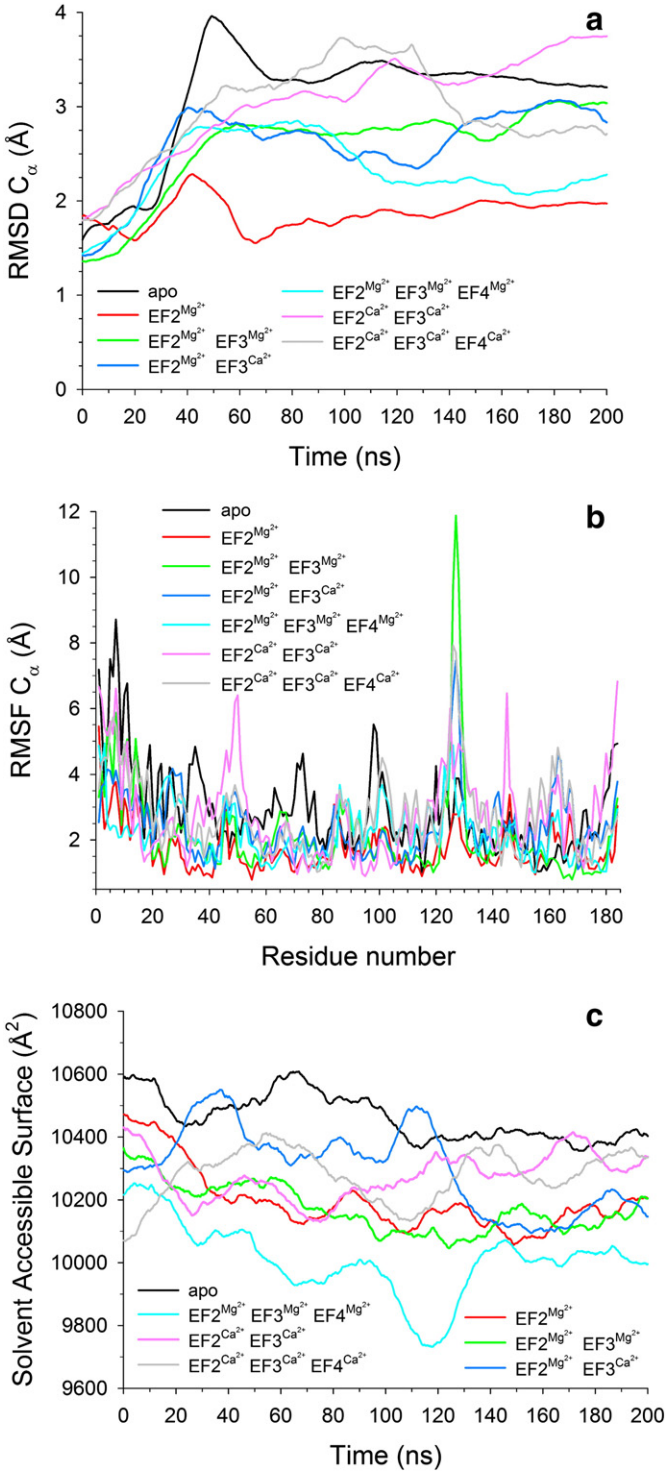

Fig. 7. Structural descriptors of mGCAP1 dynamical features calculated on the trajectories obtained by 200 ns all-atom molecular dynamics simulations. All figures have the same legend: apo black, $EF2^{Mg^{2+}}$ red, $EF2^{Mg^{2+}}$ $EF3^{Mg^{2+}}$ green, $EF2^{Mg^{2+}}$ $EF3^{Ca^{2+}}$ blue, $EF2^{Mg^{2+}}$ $EF3^{Mg^{2+}}$ $EF4^{Mg^{2+}}$ cyan, $EF2^{Ca^{2+}}$ $EF3^{Ca^{2+}}$ pink, $EF2^{Ca^{2+}}$ $EF3^{Ca^{2+}}$ $EF4^{Ca^{2+}}$ gray. (a) Smoothed curves describing the time evolution over 200 ns of the C_α-RMSD calculated with respect to the relative equilibrated structure (for raw data see Fig. S2). (b) RMSF of C_α atoms for each amino acid calculated with respect to the equilibrated structure. (c) Smoothed curves describing the time evolution over 200 ns of the SASA for each mGCAP1 state (for raw data see Fig. S3).

Overall, the conformation of EF2 and EF3 was in a closed form, very similar to that of $EF2^{Mg^{2+}}$, even though the latter had no Mg^{2+} bound to EF3. This seems to support the idea that binding of Mg^{2+} to EF3 is not essential to properly structure the EF3 loop and make GCAP1 switch to its GC activating state, although the ion occupancy of EF3 seems to be a functional requirement [19,45].

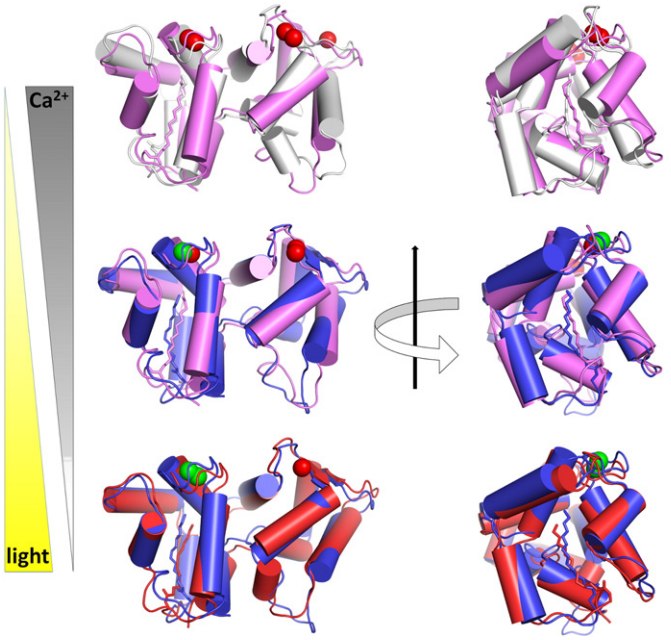

Fig. 8. Structural representation of the transition from inhibitor to activator state of mGCAP1. Left: front view, right: side view, rotated π/2 counter-clockwise. $EF2^{Ca^{2+}}$ $EF3^{Ca^{2+}}$ $EF4^{Ca^{2+}}$ inhibitor state is colored in gray, $EF2^{Ca^{2+}}$ $EF3^{Ca^{2+}}$ transition state is pink, $EF2^{Mg^{2+}}$ $EF3^{Ca^{2+}}$ transition state is blue and $EF2^{Mg^{2+}}$ activator state is red. α-Helices are represented as cylinders, β-sheets are represented by arrows, the myristoyl group is represented by sticks and Mg^{2+} and Ca^{2+} ions are represented by green and red spheres, respectively. Each structure represents the final frame after 200 ns MD simulations. C_α-RMSD values for the overlapped structures are respectively 2.8 Å (top), 2.1 Å (middle) and 2.3 Å (bottom).

3.6.5. Structural dynamics of putative GCAP1 transitory states over 200 ns simulations

The mGCAP1 state with one Mg^{2+} ion bound to EF2 and one Ca^{2+} ion bound to EF3 ($EF2^{Mg^{2+}}$ $EF3^{Ca^{2+}}$) showed a significant C_α-RMSD (2.8 Å) compared to the apo state already after equilibration. The myristoyl moiety was kinked at C4 and C8, overall inducing an S-shape in the acylic chain after equilibration. During the 200 ns MD production the myristoyl moiety was rather flexible, with kinks maintained at C7/C8, and some extended conformations observed in some frames. The 119–132 loop was quite flexible over the simulated time frame, while peculiar features of this state were: i) the short helix at the C-terminus, which closed up toward the protein interior right after the equilibration phase, and stabilized there for the whole MD production; ii) the appearance of another flexible region, namely the loop 142–149 associated to EF4; and iii) helix E in EF1 was observed to oscillate in a rigid fashion around a rather stable average position. These structural features resulted in a 2.3 Å RMSD value after the 200 ns MD production as compared to the GC activating state $EF2^{Mg^{2+}}$ (Fig. 8).

Rather different structural features characterized the other putative state of mGCAP1, namely that with two Ca^{2+} ions bound to EF2 and EF3 ($EF2^{Ca^{2+}}$ $EF3^{Ca^{2+}}$). The first difference appeared clearly after equilibration, as the C_α-RMSD (3.5 Å) compared to apo form was significantly higher than that calculated with respect to $EF2^{Mg^{2+}}$ $EF3^{Ca^{2+}}$ (2.3 Å), which maintained rather similar even at the end of 200 ns simulations (2.1 Å; Fig. 8). Binding of Ca^{2+} to both EF-hands constrained the conformation of the relative loops and made the two EF-hands interact more tightly with one another, with far reaching effects on the whole tertiary structure. Indeed, the time course of the C_α-RMSD increased monotonically (Fig. 7a), and reached the highest values in the whole set of tested

states, suggesting that this state of mGCAP1 is indeed rather unstable, and may precede $EF2^{Mg^{2+}}$ $EF3^{Ca^{2+}}$ in the time course of GCAP1 switch from GC inhibitory to activating states.

Peculiar features in the binding pocket of the myristoyl moiety were observed. The myristoyl group did not interact anymore with Leu 176 but was stabilized by interactions with Leu 80 and Tyr 76 which, compared to other cases, showed here a stronger interaction with the acylic chain. Interestingly, the C_α-RMSD calculated with respect to the $EF2^{Mg^{2+}}$ $EF3^{Mg^{2+}}$ form was 2.1 Å after equilibration, and the structures were indeed rather similar, except for the highly flexible interconnecting region 119–132 and the conformation of EF-4 at the level of the 142–148 region (E-helix and loop). Nonetheless, the $EF2^{Ca^{2+}}$ $EF3^{Ca^{2+}}$ form showed overall high local flexibilities compared to the all other forms in several structural regions, as clearly shown by the RMSF plots (Fig. 7b). This is presumably due to the fact that this transitory state serves indeed to induce to the GC the transition from inhibitor to activator states, therefore an overall flexibility may be necessary. Among the most prominent collective motions occurring during the course of the 200 ns dynamics, a slight outward tilt of helix E in EF3 was observed, as well as a rotation of the ψ angle between the peptide bond involving the myristoyl moiety and that of Gly 2, a feature already observed after equilibration. The SASA profile (Fig. 7c) highlighted already after 80 ns a higher exposition to the solvent compared to all other forms with only Mg^{2+} ions bound.

3.6.6. Structural dynamics of the GC inhibiting state over 200 ns simulations

The structure of the Ca^{2+}-saturated, holo-mGCAP1, corresponding to the GC-inhibitory state ($EF2^{Ca^{2+}}$ $EF3^{Ca^{2+}}$ $EF4^{Ca^{2+}}$) showed a C_α-RMSD of 2.7 Å with respect to the apo form after equilibration. Major differences concerned the structure of all three EF-hand calcium-binding loops, as already described in Section 3.6.2 (see Fig. 6). The C_α-RMSD with respect to the $EF2^{Ca^{2+}}$ $EF3^{Ca^{2+}}$ state after 4 ns equilibration was 2.3 Å, mostly ascribable to differences in the flexible interconnecting loop 119–132 and EF4, as expected considering that EF4 is the binding site with the lowest affinity for Ca^{2+} [18,29]. However, the structural difference increased in the time course of MD simulations, resulting in a 2.8 Å RMSD after the production phase (Fig. 8).

Analysis of MD simulations over the 200 ns showed significant variations in the N-terminal part, especially in the 2–8 strand, which caused significant changes in the amplitude of the O═C–C1–C2 dihedral angle in the myristoyl moiety, which remained stable in the 50–200 ns time frame.

Interestingly, despite the C_α-RMSD increased monotonically up to ~100 ns, reaching values among the higher ones within the tested set of mGCAP1 states (Fig. 7a), it then stabilized to values lower than those of the apo, $EF2^{Ca^{2+}}$ $EF3^{Ca^{2+}}$, $EF2^{Mg^{2+}}$ $EF3^{Mg^{2+}}$ and $EF2^{Mg^{2+}}$ $EF3^{Ca^{2+}}$ states although the SASA (Fig. 7c) was higher than the respective values for these states, except for $EF2^{Ca^{2+}}$ $EF3^{Ca^{2+}}$.

3.6.7. General conclusions from MD simulations: essential structural features for switching between different mGCAP1 regulatory states

Results from our MD simulations provide a structural interpretation that is missing so far. For instance, it provides an explanation why at least one Mg^{2+} ion has to be bound to mGCAP1 in order to switch to its activating state. Indeed, when Mg^{2+} is bound to EF2, structures are characterized by a more compact conformation, with reduced SASA compared to the inhibitory state (see Fig. 7c). The analysis also suggests another reason for apo-mGCAP1 not to exist physiologically, namely that it is characterized by high solvent accessibility (Fig. 7c) and too many regions of high flexibility (Fig. 7b). Such a state would very likely interfere with the stable and site-directed targeting to the GC. The final conformation of the myristoyl moiety is similar in both Mg^{2+}-bound activating states ($EF2^{Mg^{2+}}$ and $EF2^{Mg^{2+}}$ $EF3^{Mg^{2+}}$), and significantly differs from that of the transitory and inhibitory states.

Exchanging Mg^{2+} for Ca^{2+} in EF2 seems also a crucial step in defining the transitory state, in order to drive mGCAP1 toward its fully activating state. It is in fact apparent from MD simulations that the transitory state with two Ca^{2+} ions bound is structurally far less stable and compact than the one with one Mg^{2+} and one Ca^{2+} ion bound (Fig. 7). While our data are in agreement with Mg^{2+} being bound to EF2 in order to achieve structural features allowing the activation of the GC [21], results from MD simulations suggest that the binding of Mg^{2+} also to EF3 would cause an extreme flexibility of the 119–132 loop, and a general higher flexibility compared to the case in which the EF3 site is empty (Fig. 7a and b). On the other hand, it has been previously demonstrated that binding of a cation to EF2 is crucial for GCAP1 attachment to GC, and that in EF3 it is in fact less critical, although it enhances the efficiency of the GCAP1 docking on the target enzyme [19] and its maximal stimulation [45]. The overall moderate affinity of GCAP1 for Mg^{2+} would still allow an occupancy of EF2 by Mg^{2+} of about 55% and of EF3 of about 33% in the absence of competition with Ca^{2+} (see Supplementary Information). Moreover, the binding of GCAP1 to the GC target might stabilize its structure and reduce the intrinsic flexibility, therefore the results from our MD simulations appear substantially in line with the current model of Mg^{2+}/Ca^{2+} exchange in the regulation of GC by GCAP1 [21].

Finally, it is worth noting that besides the intrinsic differences in structural features typical of each GCAP1 regulatory state, no occurrence of dramatic conformational changes was observed in our MD simulations, the overall C_α-RMSD never exceeding 4 Å (Fig. 7). This finding is in line with a very recent work by Lim et al. [49], in which a mutant of GCAP1 lacking Ca^{2+} binding in EF4 and thus mimicking the transition to the activating state was found to have similar NMR backbone chemical shifts compared to wild type Ca^{2+}-saturated GCAP1, thus suggesting the absence of dramatic conformational changes.

A graphical summary of the dynamical features of mGCAP1 switching from the GC inhibitory state to the GC activating form is reported in Fig. 8. The figure shows a snapshot of the regulatory states after 200 ns MD simulations, in their transition toward the activating state, upon release of Ca^{2+} ions from the three EF-hands, and replacement with a Mg^{2+} ion in EF2.

4. Conclusions

By using different biophysical techniques we demonstrated that the structural effects of physiological Mg^{2+} on the regulatory state strongly depend on the specific neuronal calcium sensor. While Rec in its myristoylated form constituting the physiological condition is only slightly affected by Mg^{2+} in terms of protein structure and stability, GCAP1 and GCAP2 are both significantly affected. In particular, our results confirm that the GC activating state of GCAP1 requires the presence of at least a Mg^{2+} ion bound to the EF2 motif, a result consistent with previous biochemical investigations [45]. MD simulations further suggest a sequence of dynamical events that accompany the switch of mGCAP1 from its GC inhibitory to its activator state, which include: i) the release of a Ca^{2+} ion bound to EF4; ii) the Mg^{2+}/Ca^{2+} ion exchange in EF2; iii) and the release of a Ca^{2+} ion bound to EF3. These events accompany the structural transition toward a rather compact state, in which the myristoyl moiety shows a certain flexibility, and is eventually stabilized in a conformation that differs significantly from that of the holo, inhibitory state. It will be interesting to further investigate, whether the transition does strengthen and/or stabilize the interaction with the target GC.

The structural behavior of nm/mGCAP2 in the presence of Mg^{2+} appears significantly different from that of GCAP1, and overall rather complex. While our data clearly show that Mg^{2+} does exert an effect on the structure of both GC-activating and inhibitory states, it likely affects specific oligomeric states of GCAP2, perhaps influencing the environment of the myristic moiety in ways yet to be clarified in future studies.

Acknowledgements

We would like to thank Dr. Francesco Raimondi for his valuable technical support. This work was supported by funds from the Italian Ministry for Research and Education via Departmental funds (FUR2013) and via support from CINECA through the Italian Super Computing Resource Allocation project (ISCRA Grant: HP10CB736X to DDO) and by a grant from the Deutsche Forschungsgemeinschaft (DFG) supporting the Research Training Group GRK1885 in Oldenburg.

Appendix A. Supplementary data

Supplementary data to this article can be found online at http://dx.doi.org/10.1016/j.bbamcr.2014.10.026.

References

[1] K. Nakatani, C. Chen, K.W. Yau, Y. Koutalos, Calcium and phototransduction, Adv. Exp. Med. Biol. 514 (2002) 1–20.
[2] M.L. Woodruff, A.P. Sampath, H.R. Matthews, N.V. Krasnoperova, J. Lem, G.L. Fain, Measurement of cytoplasmic calcium concentration in the rods of wild-type and transducin knock-out mice, J. Physiol. 542 (2002) 843–854.
[3] K.W. Koch, D. Dell'Orco, A calcium-relay mechanism in vertebrate phototransduction, ACS Chem. Neurosci. 4 (2013) 909–917.
[4] K.W. Koch, T. Duda, R.K. Sharma, Ca(2+)-modulated vision-linked ROS-GC guanylate cyclase transduction machinery, Mol. Cell. Biochem. 334 (2010) 105–115.
[5] E.N. Pugh Jr., T.D. Lamb, Phototransduction in Vertebrate Rods and Cones: Molecular Mechanisms of Amplification, Recovery and Light Adaptation, Elsevier Science B.V, 2000.
[6] R. Stephen, S. Filipek, K. Palczewski, M.C. Sousa, Ca^{2+}-dependent regulation of phototransduction, Photochem. Photobiol. 84 (2008) 903–910.
[7] R.D. Burgoyne, Neuronal calcium sensor proteins: generating diversity in neuronal Ca^{2+} signalling, Nat. Rev. Neurosci. 8 (2007) 182–193.
[8] P. Philippov, K.-W. Koch, Neuronal Calcium Sensor Proteins, Nova Science Publishers, New York, 2006.
[9] J.B. Ames, R. Ishima, T. Tanaka, J.I. Gordon, L. Stryer, M. Ikura, Molecular mechanics of calcium–myristoyl switches, Nature 389 (1997) 198–202.
[10] T. Tanaka, J.B. Ames, T.S. Harvey, L. Stryer, M. Ikura, Sequestration of the membrane-targeting myristoyl group of recoverin in the calcium-free state, Nature 376 (1995) 444–447.
[11] M.E. Burns, A. Mendez, J. Chen, D.A. Baylor, Dynamics of cyclic GMP synthesis in retinal rods, Neuron 36 (2002) 81–91.
[12] A.M. Romani, A. Scarpa, Regulation of cellular magnesium, Front. Biosci. 5 (2000) D720–D734.
[13] C. Chen, K. Nakatani, Y. Koutalos, Free magnesium concentration in salamander photoreceptor outer segments, J. Physiol. 553 (2003) 125–135.
[14] W. Yang, H.W. Lee, H. Hellinga, J.J. Yang, Structural analysis, identification, and design of calcium-binding sites in proteins, Proteins 47 (2002) 344–356.
[15] E.A. Permyakov, R.H. Kretsinger, Calcium Binding Proteins, John Wiley & Sons, Hobok, New Jersey, 2011.
[16] M.E. Maguire, J.A. Cowan, Magnesium chemistry and biochemistry, Biometals 15 (2002) 203–210.
[17] I.V. Peshenko, A.M. Dizhoor, Guanylyl cyclase-activating proteins (GCAPs) are Ca^{2+}/Mg^{2+} sensors: implications for photoreceptor guanylyl cyclase (RetGC) regulation in mammalian photoreceptors, J. Biol. Chem. 279 (2004) 16903–16906.
[18] S. Lim, I. Peshenko, A. Dizhoor, J.B. Ames, Effects of Ca^{2+}, Mg^{2+}, and myristoylation on guanylyl cyclase activating protein 1 structure and stability, Biochemistry 48 (2009) 850–862.
[19] I.V. Peshenko, E.V. Olshevskaya, A.M. Dizhoor, Binding of guanylyl cyclase activating protein 1 (GCAP1) to retinal guanylyl cyclase (RetGC1). The role of individual EF-hands, J. Biol. Chem. 283 (2008) 21747–21757.
[20] T. Ozawa, M. Fukuda, M. Nara, A. Nakamura, Y. Komine, K. Kohama, Y. Umezawa, How can Ca^{2+} selectively activate recoverin in the presence of Mg^{2+}? Surface plasmon resonance and FT-IR spectroscopic studies, Biochemistry 39 (2000) 14495–14503.
[21] A.M. Dizhoor, E.V. Olshevskaya, I.V. Peshenko, Mg^{2+}/Ca^{2+} cation binding cycle of guanylyl cyclase activating proteins (GCAPs): role in regulation of photoreceptor guanylyl cyclase, Mol. Cell. Biochem. 334 (2010) 117–124.
[22] I.V. Peshenko, G.P. Moiseyev, E.V. Olshevskaya, A.M. Dizhoor, Factors that determine Ca^{2+} sensitivity of photoreceptor guanylyl cyclase. Kinetic analysis of the interaction between the Ca^{2+}-bound and the Ca^{2+}-free guanylyl cyclase activating proteins (GCAPs) and recombinant photoreceptor guanylyl cyclase 1 (RetGC-1, Biochemistry 43 (2004) 13796–13804.
[23] T. Senin II, K.E. Fischer, D.V. Komolov, P.P. Zinchenko, K.W. Philippov, Koch, Ca^{2+}-myristoyl switch in the neuronal calcium sensor recoverin requires different functions of Ca^{2+}-binding sites, J. Biol. Chem. 277 (2002) 50365–50372.
[24] K.W. Senin II, M. Koch, P.P. Akhtar, Philippov, Ca^{2+}-dependent control of rhodopsin phosphorylation: recoverin and rhodopsin kinase, Adv. Exp. Med. Biol. 514 (2002) 69–99.
[25] A. Helten, W. Saftel, K.W. Koch, Expression level and activity profile of membrane bound guanylate cyclase type 2 in rod outer segments, J. Neurochem. 103 (2007) 1439–1446.
[26] A. Helten, K.W. Koch, Calcium-dependent conformational changes in guanylate cyclase-activating protein 2 monitored by cysteine accessibility, Biochem. Biophys. Res. Commun. 356 (2007) 687–692.
[27] D. Dell'Orco, S. Sulmann, P. Zägel, V. Marino, K.-W. Koch, Impact of cone dystrophy-related mutations in GCAP1 on a kinetic model of phototransduction, Cell. Mol. Life Sci. 71 (19) (2014) 3829–3840.
[28] R. Stephen, G. Bereta, M. Golczak, K. Palczewski, M.C. Sousa, Stabilizing function for myristoyl group revealed by the crystal structure of a neuronal calcium sensor, guanylate cyclase-activating protein 1, Structure 15 (2007) 1392–1402.
[29] D. Dell'Orco, P. Behnen, S. Linse, K.W. Koch, Calcium binding, structural stability and guanylate cyclase activation in GCAP1 variants associated with human cone dystrophy, Cell. Mol. Life Sci. 67 (2010) 973–984.
[30] B. Hess, C. Kutzner, D. Van Der Spoel, E. Lindahl, GROMACS 4: algorithms for highly efficient, load-balanced, and scalable molecular simulation, J. Chem. Theory Comput. 4 (2008) 435–447.
[31] P. Bjelkmar, P. Larsson, M.A. Cuendet, B. Bess, E. Lindahl, Implementation of the CHARMM force field in GROMACS: analysis of protein stability effects from correction maps, virtual interaction sites, and water models, J. Chem. Theory Comput. 6 (2010) 459–466.
[32] A.D. Mackerell Jr., M. Feig, C.L. Brooks III, Extending the treatment of backbone energetics in protein force fields: limitations of gas-phase quantum mechanics in reproducing protein conformational distributions in molecular dynamics simulations, J. Comput. Chem. 25 (2004) 1400–1415.
[33] G. Bussi, D. Donadio, M. Parrinello, Canonical sampling through velocity rescaling, J. Chem. Phys. 126 (2007) 014101.
[34] U. Essmann, L. Perera, M.L. Berkowitz, T. Darden, H. Lee, L.G. Pedersen, A smooth particle mesh Ewald method, J. Chem. Phys. 103 (1995) 8577.
[35] B. Hess, H. Bekker, H.J.C. Berendsen, J.G.E.M. Fraaije, LINCS: a linear constraint solver for molecular simulations, J. Comput. Chem. 18 (1997) 1463–1472.
[36] H.J.C. Berendsen, J.P.M. Postma, W.F. Vangunsteren, A. Dinola, J.R. Haak, Molecular-dynamics with coupling to an external bath, J. Chem. Phys. 81 (1984) 3684–3690.
[37] M. Seeber, A. Felline, F. Raimondi, S. Muff, R. Friedman, F. Rao, A. Caflisch, F. Fanelli, Wordom: a user-friendly program for the analysis of molecular structures, trajectories, and free energy surfaces, J. Comput. Chem. 32 (2011) 1183–1194.
[38] M. Seeber, M. Cecchini, F. Rao, G. Settanni, A. Caflisch, Wordom: a program for efficient analysis of molecular dynamics simulations, Bioinformatics 23 (2007) 2625–2627.
[39] V. Marino, A. Astegno, M. Pedroni, F. Piccinelli, D. Dell'Orco, Nanodevice-induced conformational and functional changes in a prototypical calcium sensor protein, Nanoscale 6 (2014) 412–423.
[40] J. Pettelkau, I. Thondorf, S. Theisgen, H. Lilie, T. Schroder, C. Arlt, C.H. Ihling, A. Sinz, Structural analysis of guanylyl cyclase-activating protein-2 (GCAP-2) homodimer by stable isotope-labeling, chemical cross-linking, and mass spectrometry, J. Am. Soc. Mass Spectrom. 24 (2013) 1969–1979.
[41] J.Y. Hwang, K.W. Koch, The myristoylation of the neuronal Ca^{2+}-sensors guanylate cyclase-activating protein 1 and 2, Biochim. Biophys. Acta 1600 (2002) 111–117.
[42] R.E. Hughes, P.S. Brzovic, A.M. Dizhoor, R.E. Klevit, J.B. Hurley, Ca^{2+}-dependent conformational changes in bovine GCAP-2, Protein Sci. 7 (1998) 2675–2680.
[43] S. Theisgen, L. Thomas, T. Schroder, C. Lange, M. Kovermann, J. Balbach, D. Huster, The presence of membranes or micelles induces structural changes of the myristoylated guanylate-cyclase activating protein-2, Eur. Biophys. J. 40 (2011) 565–576.
[44] I.V. Peshenko, E.V. Olshevskaya, S. Lim, J.B. Ames, A.M. Dizhoor, Calcium-myristoyl Tug is a new mechanism for intramolecular tuning of calcium sensitivity and target enzyme interaction for guanylyl cyclase-activating protein 1: dynamic connection between N-fatty acyl group and EF-hand controls calcium sensitivity, J. Biol. Chem. 287 (2012) 13972–13984.
[45] I.V. Peshenko, A.M. Dizhoor, Activation and inhibition of photoreceptor guanylyl cyclase by guanylyl cyclase activating protein 1 (GCAP-1): the functional role of Mg^{2+}/Ca^{2+} exchange in EF-hand domains, J. Biol. Chem. 282 (2007) 21645–21652.
[46] I.V. Peshenko, A.M. Dizhoor, Ca^{2+} and Mg^{2+} binding properties of GCAP-1. Evidence that Mg^{2+}-bound form is the physiological activator of photoreceptor guanylyl cyclase, J. Biol. Chem. 281 (2006) 23830–23841.
[47] P. Behnen, D. Dell'Orco, K.W. Koch, Involvement of the calcium sensor GCAP1 in hereditary cone dystrophies, Biol. Chem. 391 (2010) 631–637.
[48] K. Kamenarova, M. Corton, B. Garcia-Sandoval, P. Fernandez-San Jose, V. Panchev, A. Avila-Fernandez, M.I. Lopez-Molina, C. Chakarova, C. Ayuso, S.S. Bhattacharya, Novel GUCA1A mutations suggesting possible mechanisms of pathogenesis in cone, cone-rod, and macular dystrophy patients, Biomed. Res. Int. 2013 (2013) 517570.
[49] S. Lim, I.V. Peshenko, A.M. Dizhoor, J.B. Ames, Structural insights for activation of retinal guanylate cyclase by GCAP1, PLoS One 8 (2013) e81822.